DOI:
10.2967/jnumed.115.171728

Document Version
Peer reviewed version

Journal of Nuclear Medicine, published on February 9, 2017 as doi:10.2967/jnumed.115.171728

Cardiac and respiratory motion correction for simultaneous cardiac PET-MR

Christoph Kolbitsch[1,2], Mark A. Ahlman[3], Cynthia Davies-Venn[3], Robert Evers[3], Michael Hansen[4], Devis Peressutti[1], Paul Marsden[1], Peter Kellman[4], David A. Bluemke[3] and Tobias Schaeffter[1,2]

[1]King's College London, Division of Imaging Sciences and Biomedical Engineering, London, UK

[2] Physikalisch-Technische Bundesanstalt (PTB), Abbestraße 2-12, 10587 Berlin, Germany

[3] National Institutes of Health, Clinical Center, Radiology and Imaging Sciences, Bethesda, MD, USA

[4] National Institutes of Health, National Heart, Lung, and Blood Institute, Bethesda, MD, USA,

Financial support:

Corresponding author:

Christoph Kolbitsch, Physikalisch-Technische Bundesanstalt (PTB), Medical Physics and Metrological Information Technologies, Abbestraße 2-12, 10587 Berlin, Germany,

E-mail: christoph.kolbitsch@ptb.de

Short running title:

Motion correction for cardiac PET-MR

Word count:

5211

Cardiac Positron Emission Tomography (PET) is a versatile imaging technique providing important diagnostic information about ischemic heart diseases. Respiratory and cardiac motion of the heart can strongly impair image quality and therefore diagnostic accuracy of cardiac PET scans. The aim of this study is to investigate a new cardiac PET-Magnetic Resonance (MR) approach providing respiratory and cardiac motion-compensated MR and PET images in less than five minutes. **Methods:** Free-breathing 3D MR data was acquired and retrospectively binned into multiple respiratory and cardiac motion states. 3D cardiac and respiratory motion fields were obtained with a non-rigid registration algorithm and utilized in motion-compensated MR and PET reconstructions to improve image quality. The improvement in image quality and diagnostic accuracy of the technique was assessed in simultaneous fluorodeoxyglucose (FDG) PET-MR scans of a canine model of myocardial infarct and was demonstrated in a human subject. **Results:** MR motion fields were successfully used to compensate for in-vivo cardiac motion, leading to improvements in full-width-at-half-maximum of the canine myocardium of 13±5% similar to cardiac gating but with a 90±57% higher contrast-to-noise ratio (CNR) between myocardium and blood. Motion correction led to an improvement in MR image quality in all subjects, with an increase in sharpness of the canine coronary arteries of 85±72%. A functional assessment showed very good agreement with standard MR cine scans with a difference in ejection fraction of -2±3%. MR-based respiratory and cardiac motion information was utilized to improve the PET image quality of a human in-vivo scan. **Conclusion:** The MR technique presented here provides both diagnostic and motion information which can be used to improve MR and PET image quality. Reliable respiratory and cardiac motion correction could make cardiac PET results more reproducible.

Keywords: simultaneous PET-MR, motion compensation, cardiac and respiratory motion, cardiac PET, radial phase encoding

INTRODUCTION

Cardiac PET is a highly versatile medical imaging technique (*1*,*2*), allowing for the assessment of cardiac viability or perfusion using different tracers. Recently, studies have also shown that plaque in coronary arteries can be detected by NaF PET scans (*3*). The main challenge for cardiac PET in clinical practice is the compensation of physiological motion, i.e. respiratory and cardiac movements of the heart. A range of methods has been developed in order to overcome this problem. A robust and straightforward approach is motion gating, i.e. using only data for the final image reconstruction that have been acquired in a certain motion state such as end-expiration for respiratory gating or mid-diastolic rest period for cardiac gating (*4*,*5*). The disadvantage of this approach is that only a small percentage of the acquired data is used for image reconstruction leading to a low signal-to-noise ratio. This is often compensated for by acquiring more data leading to longer scan times.

In order to utilize all the acquired data, motion correction approaches have been proposed. For this, the list-mode data is subdivided into different motion states (i.e. binned) and a motion model is used to transform these to a single reference state before combining the data. This is achieved either by combining transformed images after image reconstruction (*6*), as a pre-processing step prior to image reconstruction (*7*,*8*) or during an iterative reconstruction scheme (i.e. motion corrected image reconstruction (MCIR)) (*9*). Several techniques derive motion information directly from PET data (*7*,*8*,*10*–*12*). Nevertheless, this requires sufficient tracer uptake in the region of interest for all subdivided motion states. Anatomical imaging, such as computed tomography data has been used to overcome this limitation for respiratory motion but it has to be obtained either before or after the PET scan, which does not provide simultaneous motion information (*13*).

The introduction of simultaneous PET-MR scanners offers the possibility of using simultaneously acquired high-resolution MR information with excellent soft-tissue contrast for motion correction of PET data (*14*,*15*).

Several studies have shown that respiratory motion information obtained with MR can strongly improve the quality of PET images (*16*,*17*). Furthermore, tagged MR images have been used for cardiac motion correction in phantom experiments (*18*). However, 3D MR tagging is a time consuming technique, which has not yet found broad clinical use. Previously presented MR-techniques providing motion information for PET-MR yield either respiratory or cardiac motion information and usually no diagnostic images (*19*,*20*).

The aim of this work was to investigate a new practical MR-technique to obtain anatomical images together with respiratory and cardiac motion information in less than five minutes, which can be used for MCIR of MR images with diagnostic utility and can also be immediately applied to PET MCIR. The proposed method was evaluated in-vivo in a canine infarct model and demonstrated in in-vivo human FDG PET-MR scans. The effect of MCIR on high-resolution MR and PET image quality was assessed, i.e. localization of tracer uptake in the myocardium and CNR between myocardium and blood.

METHODS AND MATERIALS

MR and PET data were acquired simultaneously during free-breathing and without electrocardiogram synchronization in canine and human subjects. In a first step, the MR data was binned based on a respiratory self-navigator and respiratory motion was estimated (*21*). A second included respiratory motion compensation and the MR data was binned based on the electrocardiogram to determine non-rigid cardiac motion. In a final step, combined respiratory and cardiac motion

information was utilized in MCIR provided high-resolution 3D MR anatomical information and complementary 3D functional PET images. A visual summary of this approach is shown in Fig. 1.

Infarct Model

The proposed technique was evaluated in a previously established canine infarct model (*22*). Five canine subjects (10-13 months old) were imaged 58 $\pm$ 4 days after they underwent a 90-minute surgical occlusion of the left anterior descending coronary artery followed by reperfusion, which caused a subendocardial infarct and subsequent myocardial fibrosis. The main aim of the canine study was to perform multi-modality non-invasive imaging of myocardial fibrosis and to assess the sensitivity of several modalities for detecting chronic myocardial scar. The study was approved by the National Institutes of Health Animal Care and Use committee and Department of Veterinary Resources.

MR Data Acquisition

GRPE is a Cartesian sampling scheme. The phase encoding (PE) positions in the 2D PE_y-PE_z plane were obtained in a radial pattern rather than on a Cartesian grid (*23*). The angle between two successively acquired GRPE lines is the Golden angle of 111.24^o. This led to a homogenous coverage of the 2D PE plane over time and allowed for retrospective combination of data based on respiratory or electrocardiogram information. Due to the radial distribution of the PE lines, images with high quality could be reconstructed even from very few lines using iterative non-Cartesian reconstruction methods. Please also see supplemental figure 1 for more details on the data acquisition scheme.

MR In-Vivo Experiments

The GRPE trajectory was implemented on a 3T Biograph mMR (Siemens Healthcare). T1-weighted gradient echo images were acquired 5 min after IV injection of 10 mL gadofosveset using the following

imaging parameters: repetition/echo time: 4.7/2.3 ms, flip angle: 12°, field-of-view: 288 mm^3, voxel size: 1.5 mm^3 and total scan time: 4.19 min. Between three and five channels of a phased array coil were automatically selected for signal reception depending on the positioning of the canine subject. For respiratory motion estimation, data was split into eight respiratory and twelve cardiac motion states using a soft-gating approach (*24*).

Prior to GRPE standard Cartesian multi-slice 2D cine scans were acquired covering the entire left ventricle using retrospective cardiac gating during free-breathing. Respiratory motion artefacts were minimized by averaging over two consecutive acquisitions. To assess the area of fibrosis delayed enhancement multi-slice 2D images were obtained between 12 and 25 min after administration of 10 mL gadoteric acid.

All images obtained with the 3D GRPE sampling scheme were reconstructed offline using Matlab (The MathWorks, Inc., Natick, MA, USA) with a non-Cartesian iterative sensitivity encoding reconstruction scheme (*25*). The required coil sensitivity maps were calculated from the data itself. A temporal and spatial total variation constraint was included into the reconstruction of motion resolved data to utilize data redundancy and improve final image quality (*26*).

Motion Surrogates

A respiratory motion surrogate was calculated from 1D inferior-superior projections at $PE_y = PE_z = 0$ and used for self-navigation with a temporal resolution of 0.98s (*21*). Due to the limited temporal resolution of the 1D inferior-superior projections an external electrocardiogram was used as a cardiac motion surrogate.

Motion Gating and Binning

Based on these motion surrogate signals, the acquired data was separated into several different motion states. Gated images were obtained by restricting data used for the image reconstruction to a single motion state of each motion cycle, which minimizes motion artefacts.

For Cardiac gating the windows were positioned in mid-diastole covering 20% ($CG_{20\%}$) or 60% ($CG_{60\%}$) of the cardiac cycle independent of the respiratory motion state. In addition, dual-gating *(5)* was carried out restricting the data used for image reconstruction to 20% ($DG_{20\%}$) or 60% ($DG_{60\%}$) of a respiratory gating window in end-expiration and a cardiac gating window in mid-diastole leading to an image reconstruction using 4% and 36% of the total data, respectively. In addition, dual gating with a 60% respiratory and 20% cardiac gating window was applied ($DG_{60\%-20\%}$).

Respiratory binning was carried out based on the amplitude of the respiratory surrogate such that each of the eight motion bin contains the same amount of data. For cardiac binning the cardiac cycle was separated into twelve equally spaced time intervals.

MR Motion Estimation and Motion Correction

A Temporal Sparse Free Form Deformation technique was used to estimate non-rigid respiratory and cardiac motion (*27*). This technique yielded displacement fields for each pixel describing the forward and backward transformation from a reference image to all other images. Non-rigid MCIR was carried out directly during the iterative image reconstruction of the final MCIR MR images by applying motion vector fields at each iteration (*28*). The reference motion states for all image registrations were end-expiration and mid-diastole.

In addition, affine respiratory motion parameters were obtained for a region-of-interest covering the heart using a normalized cross-correlation based registration algorithm (*29*). The affine respiratory motion information was only used to speed up the reconstruction of the cardiac motion resolved images. All other MCIR reconstructions were carried out using non-rigid cardiac and non-rigid

respiratory motion information, unless stated otherwise. Affine motion correction can be carried out as a preprocessing step prior to the iterative image reconstruction, requiring less computational time than the iterative non-rigid MCIR approach.

Evaluation of MR Image Quality and Motion Accuracy

Functional parameters such as end-diastolic volume, end-systolic volume, ejection fraction and myocardial mass were measured in the cardiac motion-resolved images after respiratory motion correction.

In order to assess the accuracy of respiratory and cardiac motion correction, the sharpness of the right coronary artery was measured in reformatted MR images (*30*) without motion correction with $CG_{20\%}$ and with cardiac and respiratory MCIR. The small diameter of the coronary arteries makes them very susceptible to physiological motion and therefore they provide a sensitive measure for the performance of MCIR.

PET In-Vivo Experiments

Five canine subjects were injected IV with 370 MBq of ^{18}F-FDG 113 $\pm$ 36 min before acquiring cardiac PET list-mode data for five minutes simultaneously with the GRPE-MR scan.

PET Image Reconstruction and Motion Correction

PET images were reconstructed with STIR (Software for Tomographic Image Reconstruction) using an iterative three-dimensional ordered subsets expectation maximization algorithm with 23 subsets and two full iterations and 4 mm isotropic 3D Gaussian post-filtering (*31*). MCIR was carried out during reconstruction to transform voxels to the same motion state at each iteration, which was selected to be mid-diastole and end-expiration, respectively (*9*). Motion was only compensated for, if the motion

amplitude in the heart was larger than the MR resolution to minimize reconstruction times. The position and size of gating and binning windows were the same as for the simultaneously acquired MR data.

The MR-based attenuation correction values were acquired during free-breathing. This image is an average over multiple cardiac and respiratory cycles and describes mainly the most common cardiac and respiratory motion state, (i.e. mid-diastole and end-expiration) and therefore agrees well with the reference motion states of MCIR. All PET image reconstructions except MCIR were carried out with the unmodified attenuation correction image. For MCIR it was transformed to match the individual motion states using the MR-based motion information.

Evaluation of PET Images

The myocardial uptake was analyzed using American Heart Association 17-segment bull's-eye plots. In addition, full-width at half-maximum (FWHM) of the tracer uptake in the myocardium was measured at a mid-posterior position and basal-posterior position in reformatted short-axis slices as an average over a 10° segment. These locations showed high cardiac motion amplitudes in all dogs. CNR values were calculated at these positions as the difference between the peak myocardial signal and the mean blood-pool signal relative to the standard deviation of the blood-pool signal. The analysis was performed for uncorrected, $CG_{20\%}$ $CG_{60\%}$ and MCIR images. One-tailed paired student t-tests assuming that motion compensation improves image quality were used to compare the results considering a p value smaller than 0.01 as statistically significant.

Human In-Vivo PET-MR Scans

GRPE and PET data were obtained simultaneously in a female subject (55 years) 8 min after IV injection of 20 mL Gadobenate dimeglumine and 121 min after IV injection of 368.15 MBq of ^{18}F-FDG. This scan was part of a study to assess vasculitis approved by the National Institutes of Health

Institutional Review Board (NCT02257866). For cardiac motion-resolved images, data was split into eight cardiac motion states to ensure sufficient image quality for accurate cardiac motion estimation. The MR-based attenuation map was adapted based on the MCIR GRPE image to ensure attenuation map and MCIR PET data are in the same motion state. The MCIR MR image was used to semi-automatically redefine the lung-liver and heart-lung boundaries of the attenuation map. All other MR and PET acquisition and reconstruction parameters were the same as for the canine subjects.

RESULTS

Results are reported from canine subjects unless explicitly stated otherwise.

MR Assessment of Cardiac Function

We found good agreement between left ventricular volumes and mass measured on the free-breathing cine data set compared to the GRPE images binned into 12 cardiac phases with a difference in end-diastolic volume of -0.2±4mL, in end-systolic volume of 1±2mL, in myocardial mass of 2±8g and ejection fraction of -2±3%. Bland-Altman plots are shown in supplemental figure 2.

MR Motion Estimation

The amplitude of respiratory motion of the heart was very small with an average over all canine subjects of 0.9±0.3mm (max: 1.3mm). For cardiac motion, the motion amplitude was 5±3mm with similar amplitudes perpendicular and parallel to the axis of the left ventricle. Based on these findings, only the cardiac motion component was used for MCIR of the PET data. A visualization of cardiac motion fields can be found in supplemental figure 3.

MR Motion Correction

Figure 3 shows a comparison between uncorrected, $CG_{20\%}$ and cardiac and respiratory MCIR MR images. MCIR strongly improves image quality leading to clearly superior depiction of small features such as the wall of the myocardium and coronary arteries.

Figure 3 shows reformatted images depicting the right and left coronary arteries comparing uncorrected, $CG_{20\%}$ and MCIR MR images. An improvement in vessel sharpness of 61±77% (p=0.03) and 85±72% (p=0.006) relative to the uncorrected images was achieved with CG20% and MCIR, respectively. MCIR improved the vessel sharpness by 18±12% (p=0.012) compared to CG20%.

PET In-Vivo MCIR

The canine in-vivo PET results are depicted in Figure 4. A 2-chamber slice from the delayed enhancement MR scan shows enhancement of the inferior wall of the left ventricle. This region correlates well with low uptake in the corresponding FDG-PET scan, although PET seems to overestimate the subendocardial scar. In the bulls-eye plot, the low uptake region is clearly depicted for both the uncorrected and MCIR approach.

Cardiac motion leads to signal blurring which is visible in basal and mid-ventricular short-axis (SA) slices (Fig. 4B). The strongest blurring effect occurs in the posterior part of the ventricle. In this area the proposed MCIR approach leads to an increase of signal amplitude and an improved FWHM of the myocardial uptake of approximately 30%.

The pooled data from all five dogs is summarized in Table 1. Compared to the uncorrected images, MCIR and $CG_{20\%}$ achieved a similar improvement in FWHM (sharpness) of 13±5% (p<0.001) and 14±9% (p<0.001), respectively. MCIR resulted in a similar CNR as the uncorrected reconstruction (p=0.124) which was 90±57% (p=0.0054) higher than for CG20%. $CG_{60\%}$ did not lead to a statistically

significant improvement of FWHM compared to the uncorrected case probably due to residual systolic motion occurring in the gating window. A summary of all comparisons is given in supplemental tables 1 and 2.

Human In-Vivo MR and PET MCIR

Uncorrected and MCIR MR and PET images are shown in figure 5. Respiratory and cardiac motion fields are shown in supplemental figure 4. The maximum motion amplitudes of the heart were 16mm for respiratory and 14mm for cardiac motion. Therefore, both non-rigid respiratory and cardiac motion information were used for the final MR and PET MCIR reconstruction. MR image quality was strongly improved using MCIR. MCIR led to a better visualization of the FDG uptake in the myocardium and an increase in CNR of 103% and an improvement of FWHM of 18% compared to the uncorrected PET images. $DG_{20\%}$, $DG_{60\%-20\%}$ and $DG_{60\%}$ led to reduced CNR of -17%, -12% and -58% compared to MCIR.

DISCUSSION

In this in-vivo study we presented a practical MR technique, that yields 3D high-resolution anatomical and functional information in one 5-minute scan. Derived respiratory and cardiac motion fields allow for MR and PET MCIR, which significantly improves image quality.

The functional assessment of the left ventricle on the cardiac-motion resolved MR images showed a slight overestimation of the end-systolic volume and thus underestimation of the ejection fraction by -2$\pm$3% compared to the multi-slice 2D cine. This is probably due to the lower temporal resolution of the proposed method, which causes blurring of the fast systolic contraction. Nevertheless, the error has a similar magnitude compared to other 3D cine studies with higher resolution and scan times of 10 min (*32*). As mentioned above respiratory motion amplitudes of the canine hearts were very

small, therefore acquiring the multi-slice 2D cine data during free-breathing and averaging MR raw data over two consecutive acquisitions was considered a good gold standard.

The uptake of FDG in the human myocardium was very low, probably because the patient was fasting and underwent a PET-Computed Tomography scan prior to the PET-MR which prolonged the time between tracer application and imaging. Nevertheless, this demonstrated very well that MCIR can recover PET uptake differences (i.e. between myocardium and blood pool) which are otherwise hardly visible due to motion blurring. This could be especially important for small uptake regions such as NaF PET scans of coronary plaque (*3*). DG20% led to poor image quality due to the low number of counts which would need to be compensated for with longer acquisition times. For DG60% the gating windows were too wide and did not minimize motion artefacts sufficiently.

Changes in the subject's respiratory pattern during data acquisition can make it challenging to provide an accurate motion model for the entire scan. Further studies are required to investigate how these changes can be detected and how the motion modelling process needs to be adapted to accommodate for this situation. For this study the coil-sensitivity information was obtained from the uncorrected MR data. Further improvements in image quality might be achieved by recalculating coil-sensitivity maps after each MCIR step.

One limitation of this study is the small number of subjects and that for PET respiratory MCIR could not be evaluated in the animal model due to small respiratory amplitudes of the canine heart. However, the feasibility of MCIR simultaneous PET-MR could be demonstrated and quantified.

So far, random and scatter coincidences were not accounted for in the PET reconstruction. This will be part of future developments.

Several methods have been proposed to obtain motion information directly from FDG-PET scans (*7*,*8*,*11–13*). Nevertheless, the accuracy of the estimated motion depends, especially for non-rigid cardiac motion, on sufficient PET uptake in the ventricle. The advantage of our method is that it can

provide accurate motion information for different PET tracers independent of the uptake characteristics.

The improvement in measured uptake values of the canine myocardium was up to 24% which is in good agreement with previous human studies reporting relative differences in the activity concentration and in wall thickness measurement between 20 and 30% due to cardiac motion (*13*). Furthermore, our results suggest that MCIR achieves an improvement in FWHM of PET uptake representing an increase in resolution of up to 30%, which is comparable to $CG_{20\%}$. In contrast to cardiac gating MCIR utilizes all the available PET data and therefore leads to 90% higher CNR. In this study CG_{60}% did not lead to a statistically significant improvement in image quality compared to the uncorrected PET images.

CONCLUSION

We have presented for the first time a practical MR technique, which yields diagnostic and motion information of the heart in less than five minutes. The cardiac and respiratory motion information was successfully applied to improve the quality of MR and simultaneously acquired PET data. This approach could strongly increase image quality and diagnostic accuracy for cardiac PET studies, particularly for lesions of small size and activity.

ACKNOWLEDGEMENT

This work was supported by the SUBLIMA project (funded by the European Union under the seventh framework program, no: 241711) and by the Centre of Excellence in Medical Engineering (funded by the Wellcome Trust and EPSRC, no: WT 088641/Z/09/Z). This research was also supported in part by the National Institutes of Health intramural research training program. The authors would like to

thank Dr Kris Thielemans for his support with the PET reconstruction and Dr. Peter Grayson for collaborative work in in this study.

REFERENCES

1. Bengel FM, Higuchi T, Javadi MS, Lautamäki R. Cardiac positron emission tomography. *J Am Coll Cardiol*. 2009;54:1-15.
2. Schindler TH, Schelbert HR, Quercioli A, Dilsizian V. Cardiac PET imaging for the detection and monitoring of coronary artery disease and microvascular health. *JACC Cardiovasc Imaging*. 2010;3:623-640.
3. Joshi N V., Vesey AT, Williams MC, et al. 18F-fluoride positron emission tomography for identification of ruptured and high-risk coronary atherosclerotic plaques: a prospective clinical trial. *Lancet*. 2014;383:705-713.
4. Chander A, Brenner M, Lautamäki R, Voicu C, Merrill J, Bengel FM. Comparison of measures of left ventricular function from electrocardiographically gated 82Rb PET with contrast-enhanced CT ventriculography: a hybrid PET/CT analysis. *J Nucl Med*. 2008;49:1643-1650.
5. Teräs M, Kokki T, Durand-Schaefer N, et al. Dual-gated cardiac PET–clinical feasibility study. *Eur J Nucl Med Mol Imaging*. 2010;37:505-516.
6. Klein GJ, Reutter BW, Huesman RH. Non-rigid summing of gated PET via optical flow. *IEEE Trans Nucl Sci*. 1997;44:1509-1512.
7. Livieratos L, Stegger L, Bloomfield PM, Schafers K, Bailey DL, Camici PG. Rigid-body transformation of list-mode projection data for respiratory motion correction in cardiac PET. *Phys Med Biol*. 2005;50:3313-3322.
8. Feng T, Wang J, Fung G, Tsui B. Non-rigid dual respiratory and cardiac motion correction methods after, during, and before image reconstruction for 4D cardiac PET. *Phys Med Biol*. 2016;61:151-168.
9. Qiao F, Pan T, Clark Jr JW, Mawlawi OR. A motion-incorporated reconstruction method for gated PET studies. *Phys Med Biol*. 2006;51:3769-3783.
10. Lamare F, Ledesma Carbayo MJ, Cresson T, et al. List-mode-based reconstruction for respiratory motion correction in PET using non-rigid body transformations. *Phys Med Biol*. 2007;52:5187-5204.
11. Gigengack F, Ruthotto L, Burger M, Wolters CH, Xiaoyi Jiang, Schafers KP. Motion correction in dual gated cardiac PET using mass-preserving image registration. *IEEE Trans Med Imaging*. 2012;31:698-712.
12. Le Meunier L, Slomka PJ, Dey D, et al. Motion frozen 18F-FDG cardiac PET. *J Nucl Cardiol*. 2011;18:259-266.
13. Lamare F, LeMaitre A, Dawood M, et al. Evaluation of respiratory and cardiac motion correction schemes in dual gated PET/CT cardiac imaging. *Med Phys*. 2014;41:72504.
14. Furst S, Grimm R, Hong I, et al. Motion correction strategies forintegrated PET/MR. *J Nucl Med*. 2015;56:261-269.
15. Judenhofer MS, Wehrl HF, Newport DF, et al. Simultaneous PET-MRI: a new approach for functional and morphological imaging. *Nat Med*. 2008;14:459-465.

16. Fayad H, Schmidt H, Wurslin C, Visvikis D. Reconstruction incorporated respiratory motion correction in clinical simultaneous PET/MR imaging for oncology applications. *J Nucl Med*. 2015;56:884-890.

17. Grimm R, Fürst S, Souvatzoglou M, et al. Self-gated MRI motion modeling for respiratory motion compensation in integrated PET/MRI. *Med Image Anal*. 2015;19:110-120.

18. Huang C, Petibon Y, Ouyang J, et al. Accelerated acquisition of tagged MRI for cardiac motion correction in simultaneous PET-MR: phantom and patient studies. *Med Phys*. 2015;42:1087-1097.

19. Catana C. Motion correction options in PET/MRI. *Semin Nucl Med*. 2015;45:212-223.

20. Munoz C, Kolbitsch C, Reader AJ, Marsden P, Schaeffter T, Prieto C. MR-based cardiac and respiratory motion-compensation techniques for PET-MR imaging. *PET Clin*. 2016;11:179-191.

21. Buerger C, Clough RE, King AP, Schaeffter T, Prieto C. Nonrigid motion modeling of the liver from 3-D undersampled self-gated golden-radial phase encoded MRI. *IEEE Trans Med Imaging*. 2012;31:805-815.

22. Wu KC, Kim RJ, Bluemke D a, et al. Quantification and time course of microvascular obstruction by contrast-enhanced echocardiography and magnetic resonance imaging following acute myocardial infarction and reperfusion. *J Am Coll Cardiol*. 1998;32:1756-1764.

23. Prieto C, Uribe S, Razavi R, Atkinson D, Schaeffter T. 3D Undersampled golden-radial phase encoding for DCE-MRA using inherently regularized iterative SENSE. *Magn Reson Med*. 2010;64:514-526.

24. Johnson KM, Block WF, Reeder SB, Samsonov A. Improved least squares MR image reconstruction using estimates of k-space data consistency. *Magn Reson Med*. 2012;67:1600-1608.

25. Pruessmann KP, Weiger M, Boernert P, Boesiger P. Advances in sensitivity encoding with arbitrary k-space trajectories. *Magn Reson Med*. 2001;46:638-651.

26. Cruz G, Atkinson D, Buerger C, Schaeffter T, Prieto C. Accelerated motion corrected three-dimensional abdominal MRI using total variation regularized SENSE reconstruction. *Magn Reson Med*. 2016;75:1484-1498.

27. Shi W, Jantsch M, Aljabar P, et al. Temporal sparse free-form deformations. *Med Image Anal*. 2013;17:779-789.

28. Batchelor PG, Atkinson D, Irarrazaval P, Hill DLG, Hajnal J, Larkman D. Matrix description of general motion correction applied to multishot images. *Magn Reson Med*. 2005;54:1273-1280.

29. Buerger C, Schaeffter T, King AP. Hierarchical adaptive local affine registration for fast and robust respiratory motion estimation. *Med Image Anal*. 2011;15:551-564.

30. Etienne A, Botnar RM, Muiswinkel AMC Van, Boesiger P, Manning WJ, Stuber M. “Soap-Bubble” visualization and quantitative analysis of 3D coronary magnetic resonance angiograms. *Magn Reson Med*. 2002;48:658-666.

31. Thielemans K, Tsoumpas C, Mustafovic S, et al. STIR: software for tomographic image reconstruction release 2. *Phys Med Biol*. 2012;57:867-883.

32. Pang J, Sharif B, Fan Z, et al. ECG and navigator-free four-dimensional whole-heart coronary MRA for simultaneous visualization of cardiac anatomy and function. *Magn Reson Med*. 2014;72:1208-1217.

FIGURES

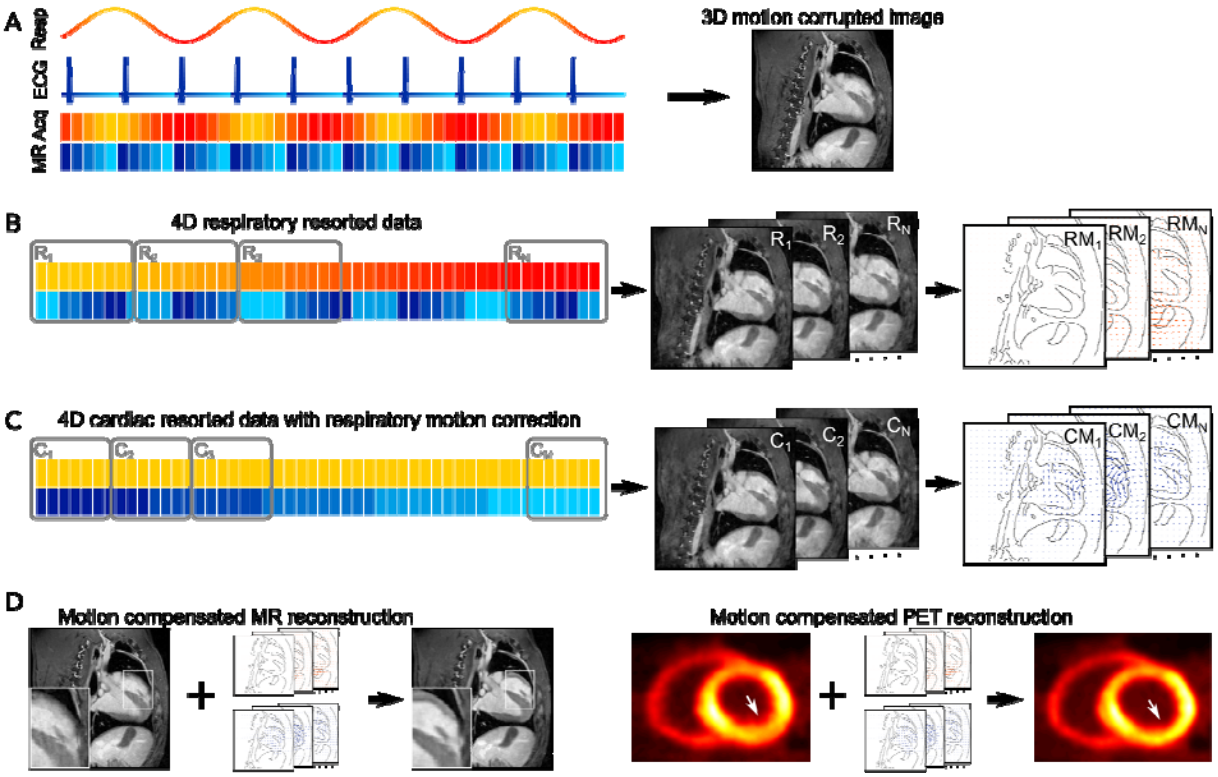

Figure 1: Overview. A 3D GRPE data is acquired during free-breathing without electrocardiogram gating over multiple respiratory and cardiac cycles. Each acquired data point is labeled with its corresponding respiratory (yellow – red) and cardiac (blue – cyan) motion state. Combining all of the data for the image reconstruction yields an image corrupted both by respiratory and by cardiac motion. **B** In a first step the data is reordered based on the respiratory labels and then 3D images (R_1 – R_N) representing N different respiratory motion states are reconstructed. An image registration algorithm is used to obtain motion fields (RM_1 – RM_N) describing the movement of the heart during breathing. **C** In a second step the acquired k-space data is transformed to the same respiratory motion state and then resorted based on the cardiac motion information. 3D images are reconstructed and non-rigid motion fields (CM_1 – CM_M) are obtained describing the motion and deformation of the heart during the cardiac cycle. **D** Respiratory and cardiac motion information can now be used for MR and PET MCIR to obtain high quality 3D images without motion artifacts.

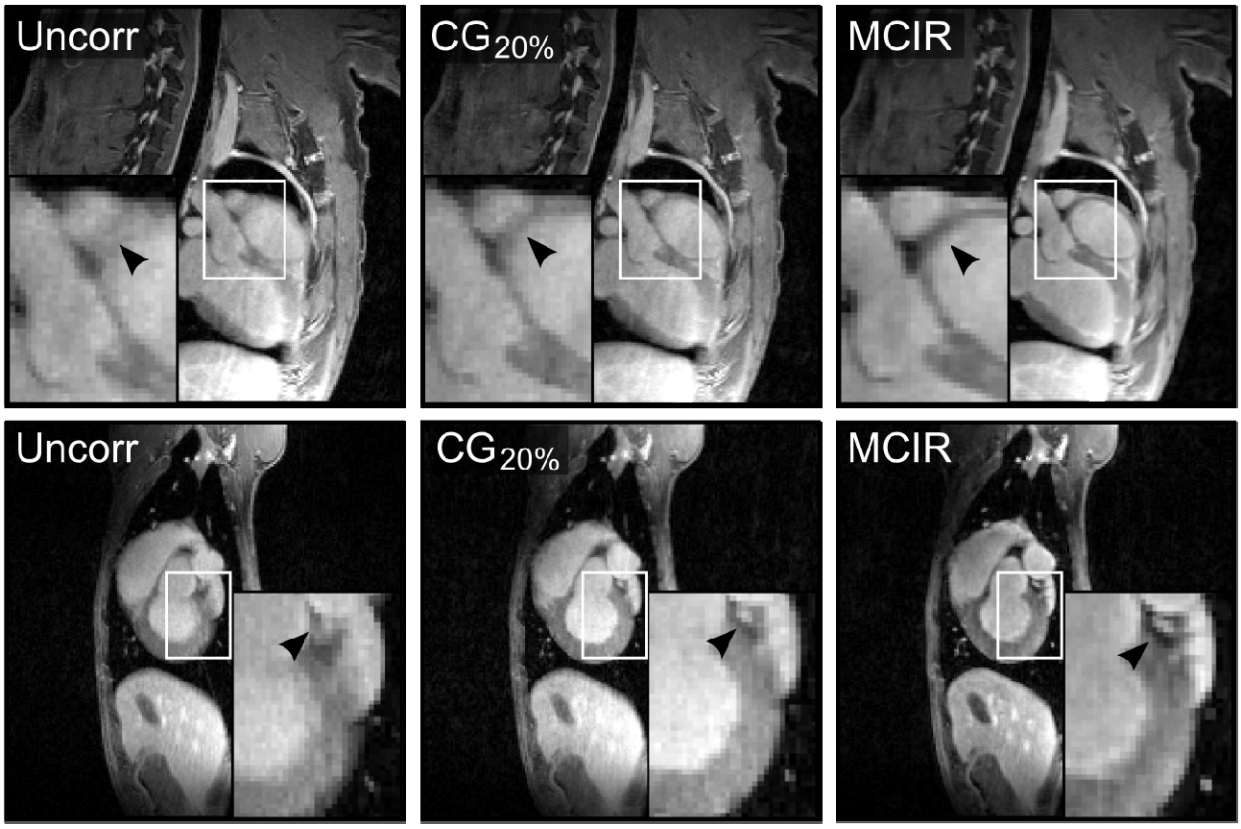

Figure 2: Results of MR MCIR. Comparison of uncorrected (Uncorr), cardiac gated ($CG_{20\%}$) and motion corrected (MCIR) MR images in two different subjects. MCIR leads to a better depiction of myocardial wall and coronary arteries (black arrows).

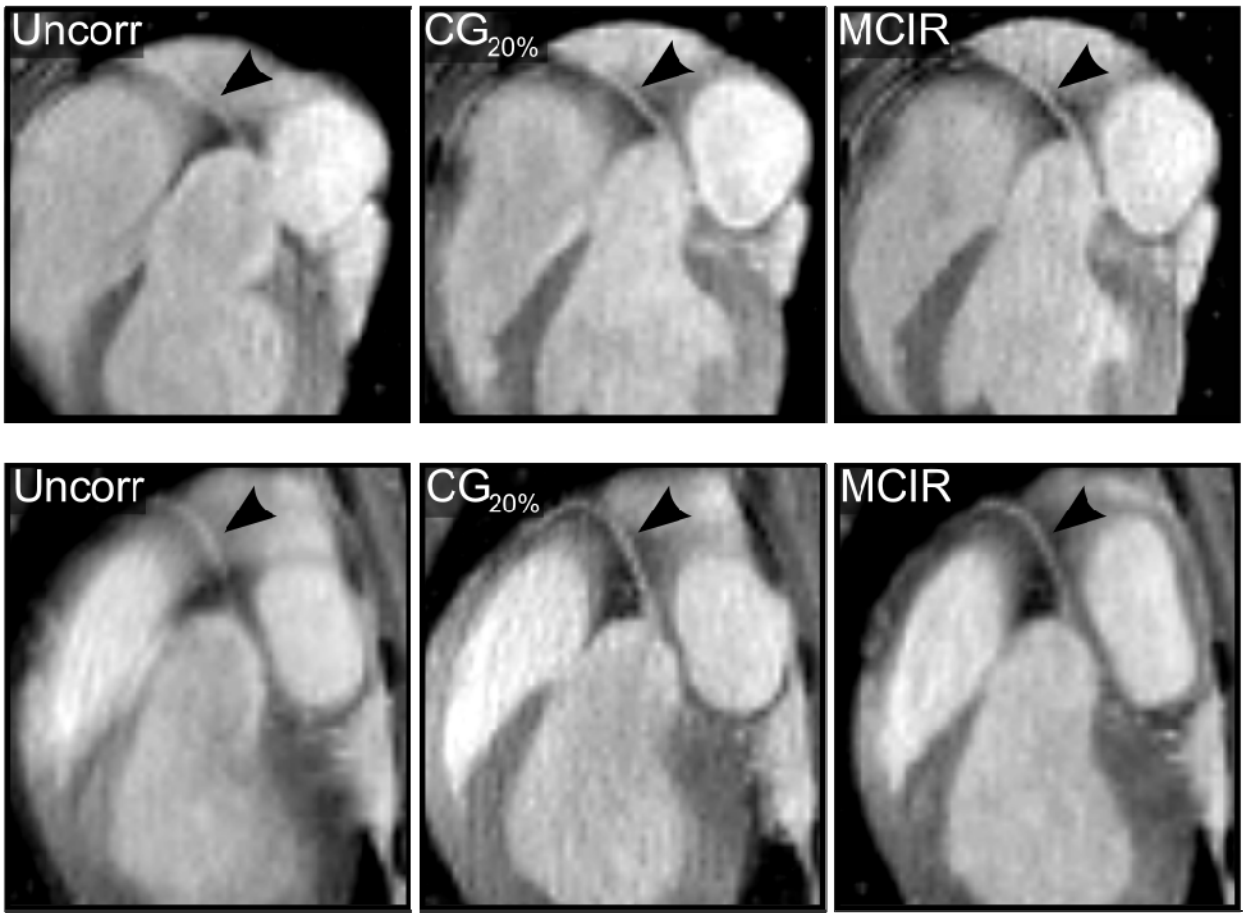

Figure 3: Assessment of coronary arteries. Reformatted images showing the right (black arrow) coronary artery for two different subjects for uncorrected (Uncorr), cardiac gated ($CG_{20\%}$) and motion corrected (MCIR) MR images.

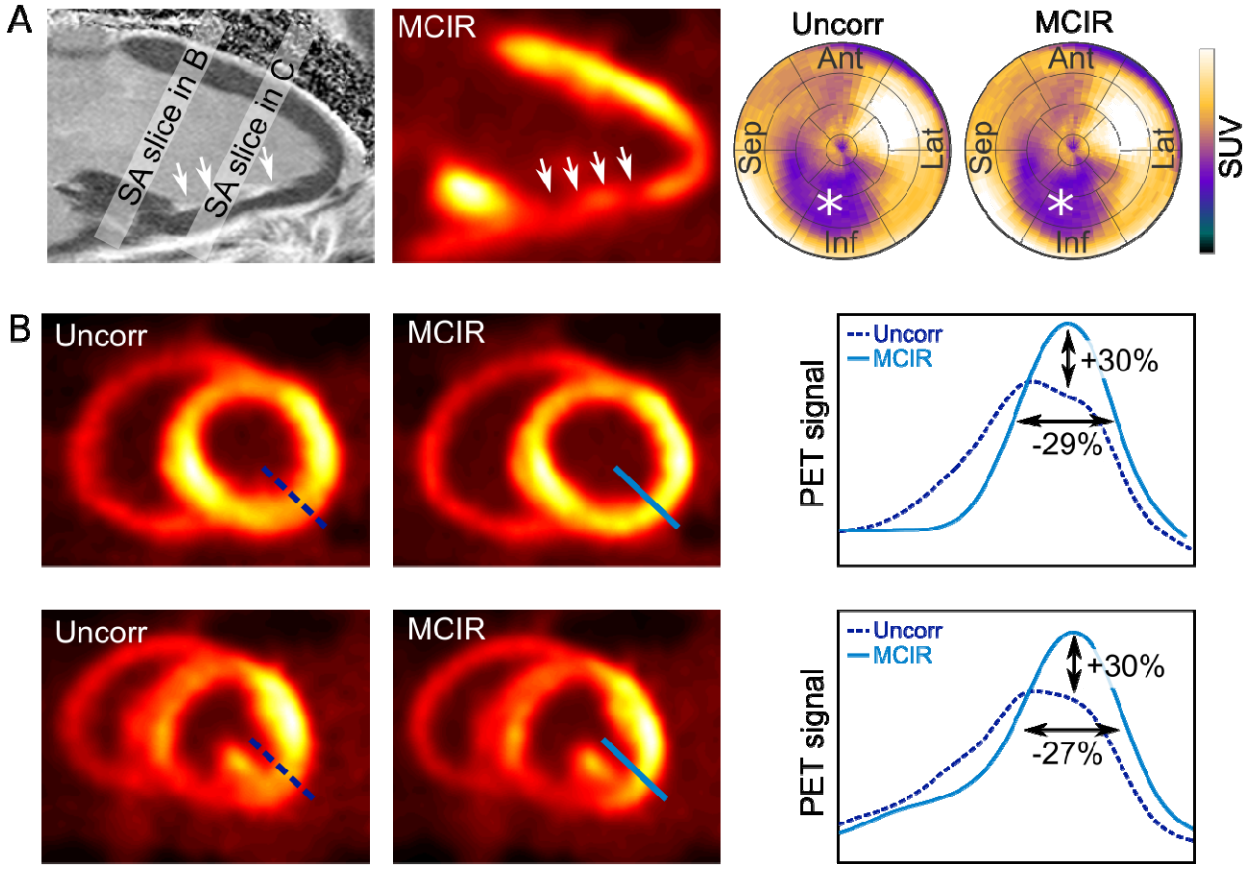

Figure 4: Results of in-vivo PET scans. A Delayed enhancement (DE) 2-chamber MR image showing fibrotic tissue in the inferior part of the left ventricle (white arrows). This area also shows low myocardial FDG uptake. Bulls-eye plots show the low uptake region clearly (*) in the uncorrected (uncorr) and cardic motion corrected (MCIR) PET images. **(B)** Basal and mid-ventricular short-axis (SA) PET motion corrupted and MCIR slices. Cardiac motion leads to strong blurring of the myocardial uptake in the posterior area of the ventricle. MCIR can correct for that leading to an increase in signal amplitude of 30% and an improvement of full-width-at-half-maximum of 29%.

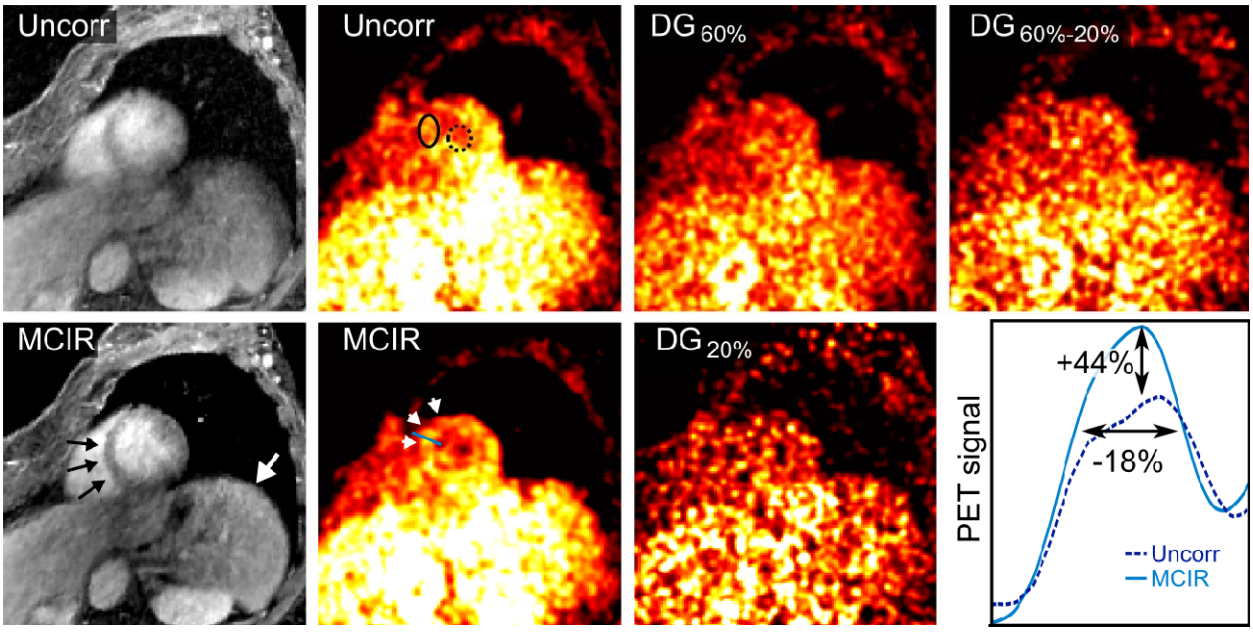

Figure 5: Results of human in-vivo PET-MR scan. Non-rigid respiratory and cardiac motion correction (MCIR) improves the visualization of myocardium (black arrow) and liver (white arrow) in the MR images. FDG uptake in the myocardium can be seen more clearly with MCIR compared to the uncorrected (Uncorr) and dual-gated (DG) images (white arrow heads). MCIR led to an improvement of CNR of 103% compared to the uncorrected images. The signal value for myocardium and blood were obtained in the solid and dotted ellipses, respectively. MCIR led to an increase in signal amplitude of 44% and an improvement of full-width-at-half-maximum of 18%.

Table 1: Results of in-vivo PET acquisitions comparing the full-width at half-maximum (FWHM) and contrast to noise ratio (CNR) at a mid-posterior (mid) and basal-posterior (bas) position in the left ventricle. The values were determined as the average over a 10° segment of the ventricle. UNC: Uncorrected, G20%: cardiac gating window in mid-diastole including 20% of the total data, G60%: cardiac gating window in mid-diastole including 60% of the total data, MCIR: cardiac motion compensation, Mean/SD: average and standard deviation over all subjects and locations.

		FWHM (mm)				CNR			
#		UNC	G60%	G20%	MCIR	UNC	G60%	G20%	MCIR
1	bas	10.53	10.95	9.13	9.57	25.82	21.69	20.65	27.76
	mid	12.89	12.56	11.72	11.63	26.33	22.43	10.41	22.06
2	bas	14.57	12.33	10.35	11.13	13.43	21.12	32.20	46.74
	mid	13.43	12.42	11.38	11.43	30.83	36.66	38.38	53.87
3	bas	13.17	12.7	11.71	11.61	22.55	18.45	23.21	31.13
	mid	12.9	12.41	11.46	11.82	49.26	48.62	42.55	77.34
4	bas	13.67	12.52	9.67	11.02	45.55	33.96	19.14	56.51
	mid	11.7	11.17	10.36	10.21	36.14	25.15	22.09	39.26
5	bas	15.69	15.52	14.77	13.91	110.62	92.04	59.34	150.23
	mid	13.83	13.77	13.77	12.4	211.33	133.13	71.53	163.84
Mean		**13.54**	**12.82**	**11.69**	**11.68**	**57.19**	**45.33**	**33.95**	**66.87**
SD		**1.13**	**1.21**	**1.64**	**1.03**	**60.55**	**37.87**	**19.32**	**50.24**

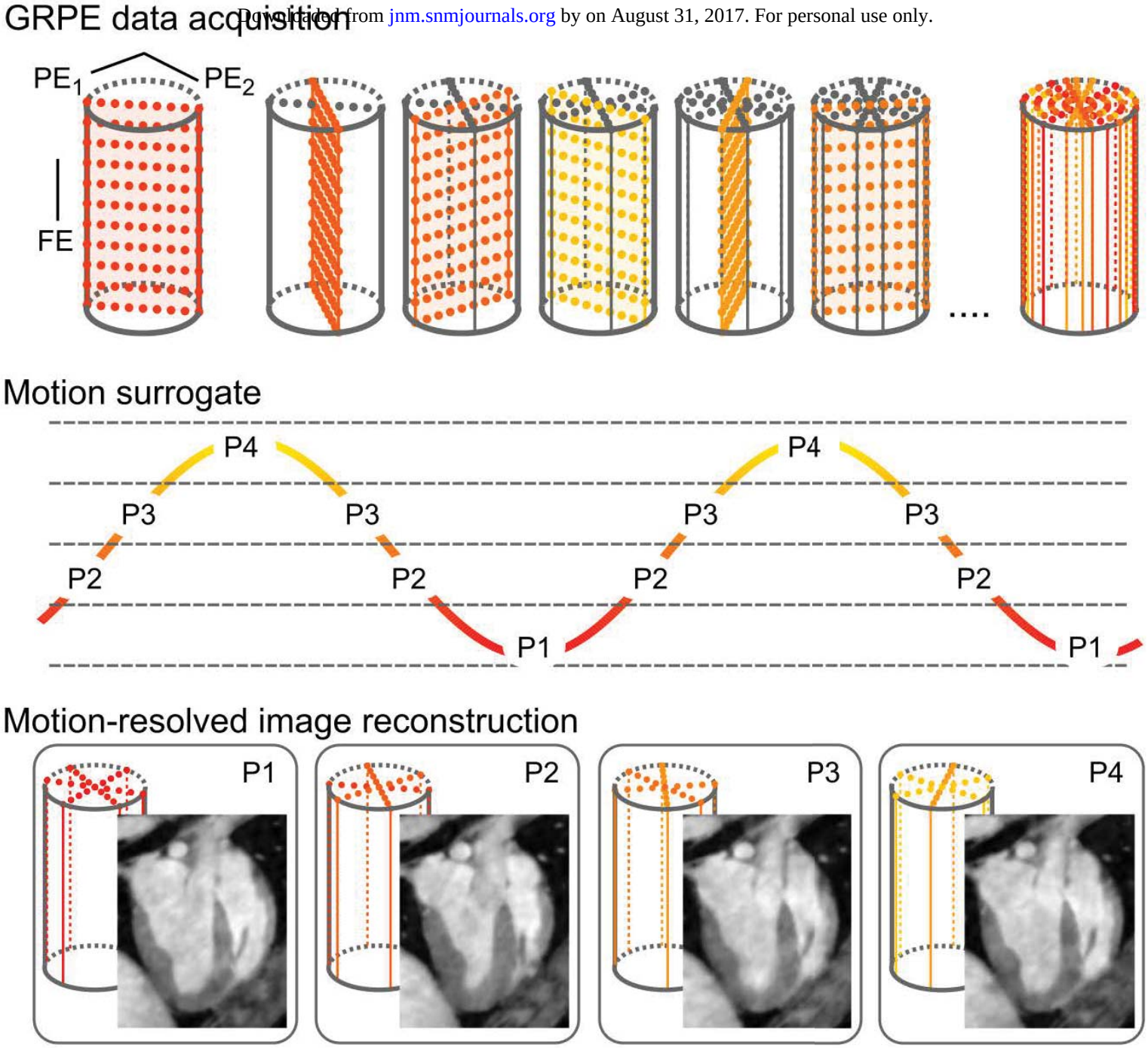

Supplemental Figure 1: Data acquisition with Golden Radial Phase Encoding (GRPE). GRPE is a 3D Cartesian sampling scheme with a Cartesian readout along the frequency encoding (FE) direction. The phase encoding points are located on radial lines in the 2D phase encoding plane (PE_1 – PE_2). The angle between subsequent lines is the golden angle leading to a homogeneous filling of the 2D PE_1 – PE_2 plane over time. Physiological signals (i.e. from external electrocardiogram) can be used to label the acquired data depending on their motion state (P1 – P4). Data acquired in the same motion state can be retrospectively binned yielding motion resolved 3D images. Due to the sampling properties of GRPE, the k-space data in each bin is homogenously distributed and a high image quality can be achieved using iterative image reconstruction schemes.

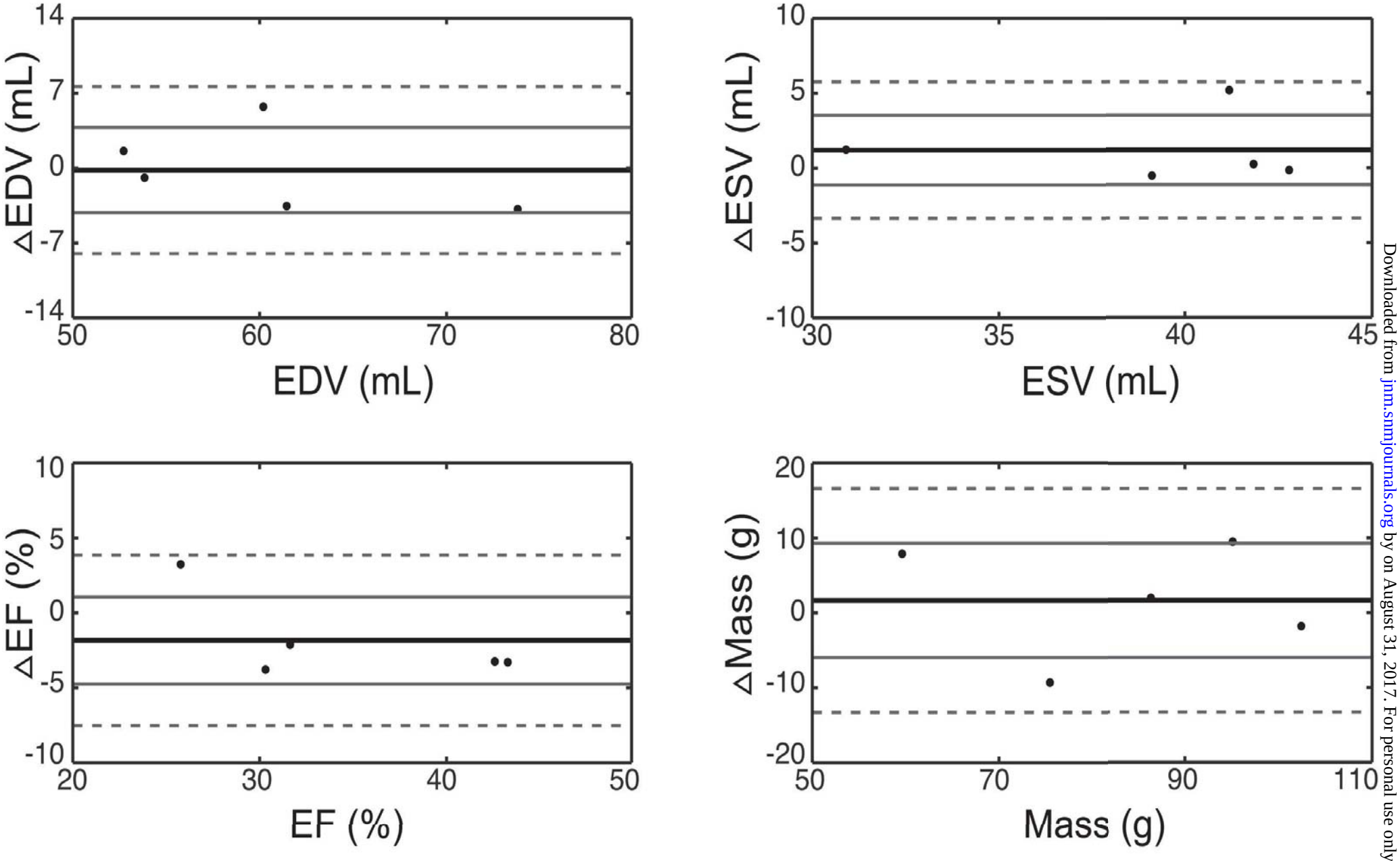

Supplemental Figure 2: Functional assessment. The functional assessment of the left ventricle shows excellent agreement between the Cartesian cine scan and the proposed method for end-diastolic volume (EDV), end-systolic volume (ESV), ejection fraction (EF) and myocardial mass (Mass).

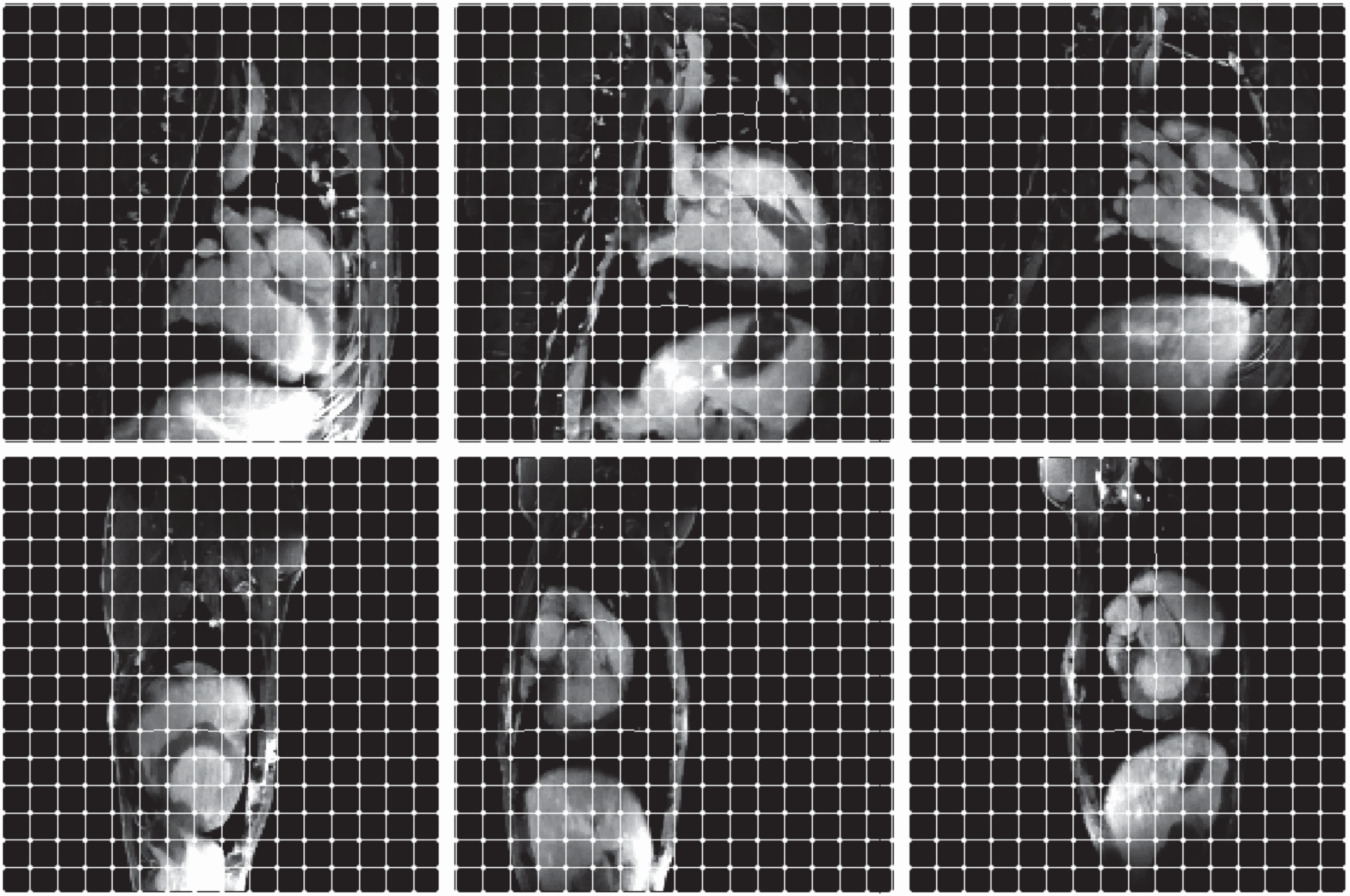

Supplemental Figure 3: Overlay of motion grids deformed by estimated non-rigid cardiac motion fields on cardiac binned MR images for three different canine subjects. The motion grid follows the cardiac motion of the heart very well, suggesting accurate motion estimation. It is important to note that the motion grid is calculated in 3D but only a 2D intersection is shown which does not visualize motion perpendicular to the visualized image plane.

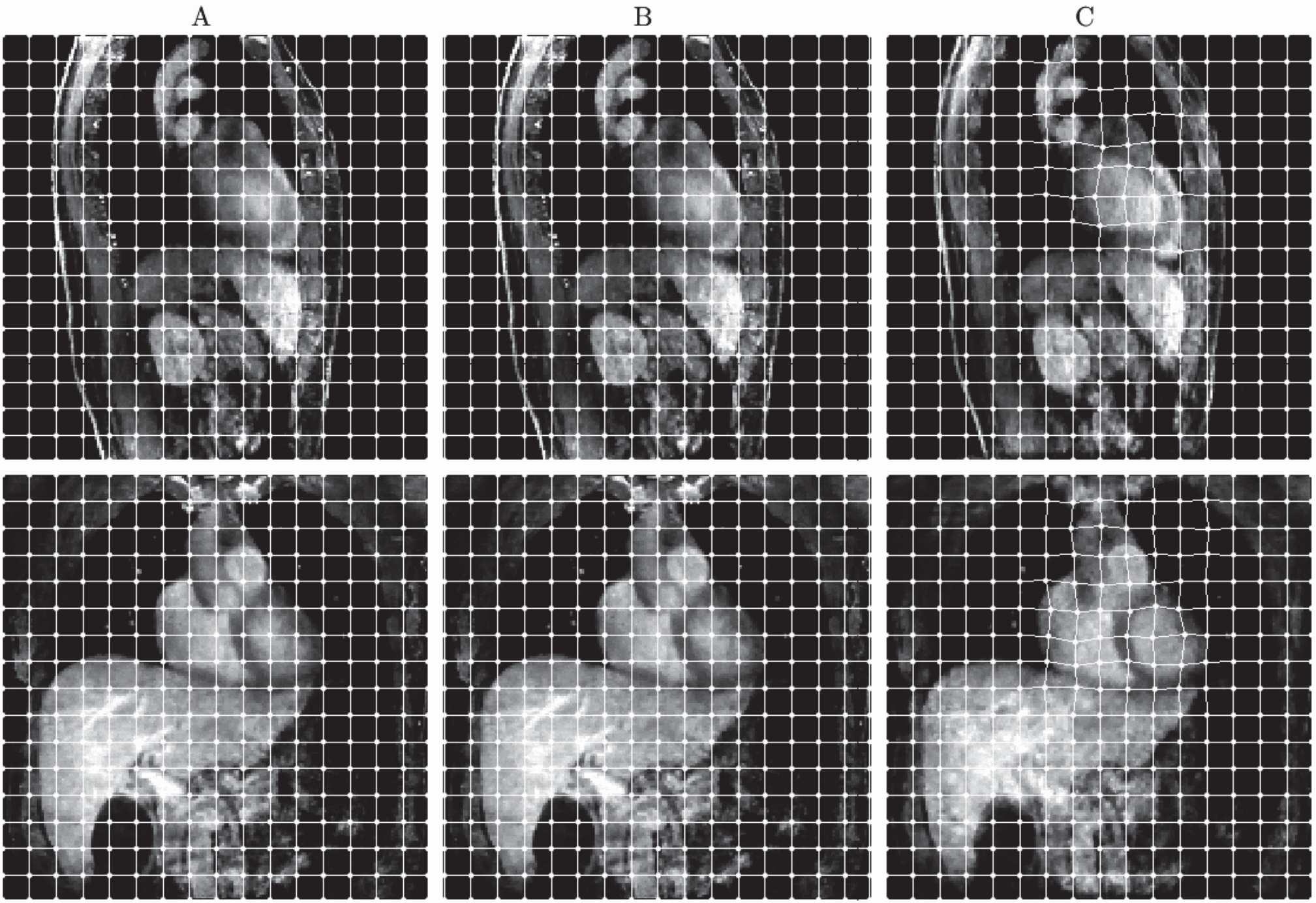

Supplemental Figure 4: Overlay of motion grids deformed by estimated motion fields on cardiac/respiratory binned MR images for a human subject. A: Affine respiratory motion fields, B: Non-rigid respiratory motion fields, C: Non-rigid cardiac motion fields.

Supplemental Table 1: Results of in-vivo PET acquisitions comparing the relative difference of full-width at half-maximum (ΔFWHM) at a mid-posterior (mid) and basal-posterior (bas) position in the left ventricle. The values were determined as the average over a 10° segment of the ventricle. All differences are given relative to the uncorrected case, except for ΔFWHM(MCIR – $CG_{20\%}$) and ΔFWHM(MCIR – $CG_{60\%}$) where the difference is relative to $CG_{20\%}$ and $CG_{60\%}$, respectively. A paired student t-test was used to determine statistical significance ($p < 0.01$, results marked in bold). UNC: Uncorrected, $CG_{20\%}$: cardiac gating window in mid-diastole including 20% of the total data, $CG_{60\%}$: cardiac gating window in mid-diastole including 60% of the total data, MCIR: cardiac motion compensation, Mean/Std: average and standard deviation over all subjects and locations.

		ΔFWHM				
		$CG_{20\%}$ - UNC	$CG_{60\%}$ - UNC	MCIR - UNC	MCIR – $CG_{20\%}$	MCIR – $CG_{60\%}$
Subject 1	bas	-13.30%	3.99%	-9.12%	4.82%	-12.60%
	mid	-9.08%	-2.56%	-9.78%	-0.77%	-7.40%
Subject 2	bas	-28.96%	-15.37%	-23.61%	7.54%	-9.73%
	mid	-15.26%	-7.52%	-14.89%	0.44%	-7.97%
Subject 3	bas	-11.09%	-3.57%	-11.85%	-0.85%	-8.58%
	mid	-11.16%	-3.80%	-8.37%	3.14%	-4.75%
Subject 4	bas	-29.26%	-8.41%	-19.39%	13.96%	-11.98%
	mid	-11.45%	-4.53%	-12.74%	-1.45%	-8.59%
Subject 5	bas	-5.86%	-1.08%	-11.34%	-5.82%	-10.37%
	mid	-0.43%	-0.43%	-10.34%	-9.95%	-9.95%
Mean		**-13.59%**	-4.33%	**-13.14%**	1.11%	**-9.19%**
Std		**9.16%**	5.25%	**4.89%**	6.74%	**2.28%**
p-value		**<0.001**	0.014	**<0.001**	0.5	**<0.001**

Supplemental Table 2: Results of in-vivo PET acquisitions comparing the relative difference of contrast to noise ratio (ΔCNR) at a mid-posterior (mid) and basal-posterior (bas) position in the left ventricle. The values were determined as the average over a 10° segment of the ventricle. All differences are given relative to the uncorrected case, except for ΔCNR(MCIR – $CG_{20\%}$) and ΔCNR(MCIR – $CG_{60\%}$) where the difference is relative to $CG_{20\%}$ and $CG_{60\%}$, respectively. A paired student t-test was used to determine statistical significance ($p < 0.01$, results marked in bold). UNC: Uncorrected, $CG_{20\%}$: cardiac gating window in mid-diastole including 20% of the total data, $CG_{60\%}$: cardiac gating window in mid-diastole including 60% of the total data, MCIR: cardiac motion compensation, Mean/Std: average and standard deviation over all subjects and locations.

		ΔCNR				
		$CG_{20\%}$ - UNC	$CG_{60\%}$ - UNC	MCIR - UNC	MCIR – $CG_{20\%}$	MCIR – $CG_{60\%}$
Subject 1	bas	-20.02%	-16.00%	6.99%	25.61%	27.99%
	mid	-60.46%	-14.81%	-19.36%	111.91%	-1.65%
Subject 2	bas	139.76%	57.26%	71.27%	45.16%	121.31%
	mid	24.49%	18.91%	42.77%	40.36%	46.94%
Subject 3	bas	2.93%	-18.18%	27.56%	34.12%	68.73%
	mid	-13.62%	-1.30%	36.31%	81.76%	59.07%
Subject 4	bas	-57.98%	-25.44%	19.39%	195.25%	66.40%
	mid	-38.88%	-30.41%	7.95%	77.73%	56.10%
Subject 5	bas	-46.36%	-16.80%	26.37%	153.17%	63.22%
	mid	-66.15%	-37.00%	-28.99%	129.05%	23.07%
Mean		-13.63%	-8.38%	19.03%	**89.41%**	**53.12%**
Std		61.40%	27.82%	29.37%	**56.79%**	**32.98%**
p-value		0.07	0.08	0.12	**0.005**	**0.0012**

The Journal of NUCLEAR MEDICINE

Cardiac and respiratory motion correction for simultaneous cardiac PET-MR

Christoph Kolbitsch, Mark A Ahlman, Cynthia Davies-Venn, Robert Evers, Michael Hansen, Devis Peressutti, Paul Marsden, Peter Kellman, David A Bluemke and Tobias Schaeffter

J Nucl Med.
Published online: February 9, 2017.
Doi: 10.2967/jnumed.115.171728

The Journal of Nuclear Medicine is published monthly.
SNMMI | Society of Nuclear Medicine and Molecular Imaging
1850 Samuel Morse Drive, Reston, VA 20190.
(Print ISSN: 0161-5505, Online ISSN: 2159-662X)

SNMMI SOCIETY OF NUCLEAR MEDICINE AND MOLECULAR IMAGING